Colloid Polym Sci (2012) 290:1537–1546
DOI 10.1007/s00396-012-2684-0

ORIGINAL CONTRIBUTION

Hofmeister effects on the colloidal stability of poly(ethylene glycol)-decorated nanoparticles

Leandro S. Blachechen · Jaqueline O. Silva · Leandro R. S. Barbosa · Rosangela Itri · Denise F. S. Petri

Received: 29 February 2012 / Revised: 8 May 2012 / Accepted: 10 May 2012 / Published online: 26 May 2012

Abstract The colloidal stability of poly(ethylene glycol)-decorated poly(methyl methacrylate), PMMA/Tween-20, particles was investigated by means of phase separation measurements, in the presence of sodium fluoride (NaF), sodium chloride, sodium bromide, sodium nitrate, or sodium thiocyanate (NaSCN) at 1.0 mol L^{-1}. Following Hofmeister's series, the dispersions of PMMA/Tween-20 destabilized faster in the presence of NaF than with NaSCN. After the phase separation, the systems were homogenized and except for the dispersions in NaF, redispersed particles took longer to destabilize, indicating that anions adsorbed on the particles, creating a new surface. Except for F^- ions, the adsorption of anions on the polar outmost shell was evidenced by means of tensiometry and small-angle X-ray scattering measurements. Fluoride ions induced the dehydration of the polar shell, without affecting the polar shell electron density, and the formation of very large aggregates. A model was proposed to explain the colloidal behavior in the presence of Hofmeister ions.

Keywords Colloidal stability · Surface tension · SAXS · Hofmeister series ions · Poly(ethylene glycol) · Latex particle

Electronic supplementary material The online version of this article (doi:10.1007/s00396-012-2684-0) contains supplementary material, which is available to authorized users.

L. S. Blachechen · J. O. Silva · D. F. S. Petri (✉)
Instituto de Química, Universidade de São Paulo,
05508-000 São Paulo, Brazil
e-mail: dfsp@usp.br

L. R. S. Barbosa · R. Itri
Instituto de Física, Universidade de São Paulo,
São Paulo, Brazil

Introduction

More than one century ago, Hofmeister observed the ability of some ions to induce protein aggregation more efficiently than others [1]. Originally, the effects of Hofmeister ions were attributed to perturbations of bulk water properties and macromolecule hydration. However, nowadays, it is commonly accepted that these two factors both contribute to the Hofmeister effects. The colloidal behavior might be affected by specific interactions between ions and macromolecules and their first hydration shell [2–5], which involve the relative polarizabilities of the ions [6], and by changes in the Hamaker constant for particle–particle interaction and in the ion hydration layer [7–9]. Considering that literature offers excellent reviews covering this topic [2–5], here, we just summarize some relevant aspects related to Hofmeister ions. Ions were ordered in the so-called Hofmeister's series, where ions that destabilize folded proteins and cause "salting-in" effect are called chaotropes or "water structure breaker" ions; SCN^- and Ba^{2+} ions are the strongest chaotrope ones of the series. Chaotropes are usually large and present high polarizabilities. Consequently, they have weak electric fields, losing their hydration layer easily. In contrast, ions which tend to stabilize proteins and cause "salting-out" effects are called kosmotropes or "water structure makers"; citrate and $(CH_3)_4N^+$ ions are the strongest kosmotropes of the series. Usually, kosmotropes are small and present low polarizabilities. Since they have high electric fields at short distances, they do not lose their hydration layer easily. Another general aspect of the series is that anions tend to be more efficient than the cations. The anions series is often found as:

$$\text{Citrate} > CO_3^{2-} > SO_4^{2-} > H_2PO_4^- > F^- > Cl^- > Br^- > NO_3^- > I^- > ClO_4^- > SCN^-$$

where kosmotropes and chaotropes are on the left and on the right, respectively.

In this study, we investigated the effect of monovalent ions, F^-, Cl^-, Br^-, NO_3^-, and SCN^-, on the colloidal stability of poly(methyl methacrylate)-Tween-20 (PMMA/Tween-20) particles by dispersion phase separation analysis. Because the hydrophilic part of Tween-20 is poly(ethylene glycol) (PEG), the incorporation of Tween-20 provided decoration of the nanoparticles with PEG. These particles were successfully used for immobilization of lectin and other proteins and further applied in quick agglutination tests for dengue fever detection [10]. Their stability in the presence of different Hofmeister anions, nevertheless, remains so far unexplored. PMMA/Tween-20 particles were synthesized by means of emulsion polymerization using poly(ethylene glycol) sorbitan monolaurate, a surfactant commercially known as Tween-20 [11]. At the end of PMMA polymerization, all surfactant molecules are on the particle surfaces with the polar head oriented to the aqueous medium and hydrophobic tail buried in the polymeric core. In fact, PMMA/Tween-20 particles and Tween-20 micelles have similar structures, namely, a hydrophobic core and a hydrophilic poly(ethylene glycol) shell. It is, however, important to note that (a) the Tween 20 micelles are approximately 50 fold smaller than the polymeric particles and (b) the Tween-20 micelles are free to break and reform with high kinetic rate constants [12] while the polymer chains in the particles are internally cross-linked. Despite of these differences, the behavior of PMMA/Tween-20 particles and Tween-20 micelles in the presence of Hofmeister salts may still be reasonably comparable, thanks to the similar PEG outer layer.

Although phase separation analysis is a reliable method for the observation of macroscopic phase separation, it does not yield information at molecular level. Thus, in order to gain insight at the molecular level about the effects of monovalent anions on the colloidal stability of PMMA/Tween-20 particles, we used Tween-20 micelles to mimic the polymer particles and investigated their colloidal behavior in the presence of the same ions by means of tensiometry and small-angle X-ray scattering. Such techniques provide information about structural changes and specific interactions at molecular level but are not adequate for large colloidal particles such as PMMA/Tween-20.

Experimental section

Materials

Methyl methacrylate (MMA; Fluka, Buchs, Switzerland), potassium persulfate ($K_2S_2O_8$; Merck Munich, Germany), and poly(ethylene glycol) sorbitan monolaurate (Tween-20; Sigma-Aldrich Co., Milwaukee, WI, USA) were used in the polymerization. Tween-20 molecule carries 20 ethylene glycol monomers distributed in the main structure and in tree branches located at the headgroup, as schematically shown in Supporting Material. Sodium chloride (NaCl; CAAL Ltda., São Paulo, Brazil), sodium fluoride (NaF; E. Merck AG-Darmstadt, Germany), sodium bromide (NaBr), sodium nitrate ($NaNO_3$), and sodium thiocyanate (NaSCN) supplied by Labsynth Ltda, São Paulo, Brazil, were used in the colloidal stability tests. All reagents were used as received.

Synthesis of PMMA/Tween-20 particles

The particles were synthesized following a typical emulsion polymerization recipe [13]. Tween-20 concentration was 60 mg L^{-1} (4.8×10^{-5} mol L^{-1}), which is close to Tween-20 critical micelle concentration (c.m.c.). The medium was purged with N_2 during the whole process and the polymerization was carried out under reflux and mechanical stirring at 500 rpm. The temperature was set to (75±2) °C, then, 10 mL of MMA were added and the temperature was brought up to (80±2) °C. Afterwards, 1.0 g of $K_2S_2O_8$, the initiator, was added. After 3 h, the system was cooled to room temperature and dialyzed (dialysis membrane 14,000 MW, Viskase Corporation, USA) against water with changes until the conductivity of dialysis water reached 5 μS cm^{-1}.

Particle characterization

The particle characterization was performed with dialyzed dispersions. Dynamic Light Scattering (DLS) and ζ-potential measurements were performed in a commercial instrument Zetasizer NanoZS (Malvern, UK). A He-Ne laser was used as a light source with wavelength λ=633 nm. Concerning the DLS experiments, the intensity of light scattered was recorded at an angle of 90° with an avalanche photodiode detector. We used the Zetasizer Software 6.2 (provided by Malvern) to determine the particle size distribution. In few words, the software uses the correlation function to obtain the distributions of the decay rates, and hence, the apparent diffusion coefficients. Finally, the distributions of the hydrodynamic radius of the scattering particles in solution are calculated via Stokes–Einstein equation [14, 15]. ζ-Potential measurements were conducted on sample-filled capillary cells and data were analyzed with the Smoluchowski equation $\xi=\mu\eta / \varepsilon$, where η is the medium viscosity and ε the medium dielectric constant. It is important to mention that such equation is only valid for spherical particles. The measurements were performed for stock dispersions of PMMA/Tween-20 diluted 100 times in Milli-Q water and for Tween-20 solutions at 1 mmol L^{-1}, which corresponds to approximately 10 times the c.m.c. value.

Scanning electron microscopy (SEM) analyses were performed to determine the morphology and mean diameter of dried particles using a SEM-FEG JEOL 7401F equipment.

The stock dispersions of PMMA/Tween-20 were diluted 100 times in Milli-Q water; then droplets were deposited onto clean Si wafers. The water evaporated slowly at room temperature. The dried dispersions were not coated prior to the analysis. The mean diameter and diameter distribution were determined with ImageJ free software over 650 dried particles.

The solid content was determined by gravimetric analysis upon drying 1 mL dispersion. The conversion of monomer into polymer (polymerization yield) was calculated based on the monomer content in 1 mL of the initial emulsion (m_I) and dried solid content in 1 mL of the final dispersion (m_F). The relation m_F/m_I gives the polymerization yield. The mean particle number density (N_P) was calculated considering the particle mean diameter calculated by DLS and the solid content, as described elsewhere [16].

Colloidal stability tests

The stability of the PMMA/Tween20 dispersion in the absence of salt and in the presence of NaF, NaCl, NaBr, $NaNO_3$, and NaSCN was studied using a separation analyzer LUMiReader®414 Separation Analyser (L.U.M. GmbH, Germany). Only salts containing the same cation, namely Na^+, were used in order to investigate the effects of anion type on the colloidal stability. Dispersions and salt solution were mixed so that final N_P was (2.7±0.2) 10^{12} particles mL^{-1} and salt concentration was 1.0 mol L^{-1}. The measurements were carried out at 30±2 °C immediately after mixing the dispersion and salt solution. The phase separation behavior was monitored by the SEP View 4.01 software, which registered the normalized integral light transmission as a function of time. Cuvettes made of polycarbonate, 2.0 mm thick and 20 mm long were used for the experiments. At the beginning, the dispersion is homogeneous and the transmitted light through the cuvette is very low. As time goes by, the dispersion starts to destabilize, fluctuations in concentration cause particles to nucleate and to aggregate. When the aggregates become large enough, they sediment, accumulating at the bottom of the cuvette and increasing the transmission of light through the upper liquid. After phase separation, the samples, still inside the cuvette, were shaken manually for a few seconds. It was enough to re-disperse the system and to obtain a homogeneous dispersion again. The re-dispersed system was analyzed again at 30±2 °C. A time interval of 45 min was arbitrarily taken between the first phase separation analysis and the re-dispersion followed by analysis.

Small-angle X-ray scattering

Small-angle X-ray scattering (SAXS) experiments were carried out at the National Laboratory of Synchrotron Light (Campinas, Brazil) at room temperature of 22±1 °C, with radiation wavelength λ=1.608 Å. Tween-20 solutions at the concentration of 1.0 and 2.0 mmol L^{-1} were measured in the absence of salt. The corresponding scattering curves resulted to be identical when normalized by the Tween-20 concentrations (data not shown). Then, the SAXS measurements in the presence of either NaSCN or NaF 1.0 mol L^{-1} were done using Tween-20 at 1.0 mmol L^{-1}. Samples were set between two mica windows, 1-mm spacer, handled in a liquid sample-holder. This was placed perpendicular to the incident X-ray beam. Each solution was measured twice with time acquisition of 10 min each run. The data presented here correspond to the average of the two sets of measurements. No radiation damage was observed during the data acquisition. The obtained curves were corrected for detector homogeneity (one-dimension position sensitive detector) and proper corrections have been carried out for the decrease of the X-ray beam intensity during the experiment. The scattering curve of the solvent was subtracted from the sample's scattering taking into account the corresponding X-ray absorption. The SAXS measurements for Tween-20 in the presence of NaCl 1.0 mol L^{-1} did not suffer a significant decrease of the scattering signal due to absorption edge at the wavelength used.

The SAXS intensity (I(q)) of an isotropic solution of monodisperse particles of low anisometry (ratio between the largest and the shortest particle axis), can be described as [17–19]

$$I(q) = k\, P(q)S(q) \quad (1)$$

where $k=\gamma\, n_p\, (\Delta\rho)^2 V^2$; γ is a factor related to the instrumental effects, n_p corresponds to the particle number density; $\Delta\rho$ is the electron density contrast between the scattering particle and the medium and V is the scattering particle volume. P(q) and S(q) correspond, respectively, to the orientational average of the scattering particle form factor and to the interparticle interference factor ($q=4\pi\sin\theta/\lambda$ is the modulus of the scattering vector and 2θ is the scattering angle). In our case, the micelle form factor P(q) is better represented by a prolate ellipsoid made up of two shells of different electron densities ρ in respect to the solvent electron density [20, 21] (in our case, $\rho_w=0.333$ e/Å^3 for aqueous solution). Accordingly, the prolate micelle, with axial ratio ν, is represented by a hydrophobic paraffinic core with electron density $\rho_{par}=0.275$ e/Å^3, and of which the shortest semi-axis length is associated to the parameter R_{par}, and the longest semi-axis length to νR_{par}. Such a hydrophobic core is thus surrounded by a polar shell of thickness σ and electron density ρ_{pol}, which includes the polar head groups and hydration water.

S(q) in Eq. 1 was calculated through the well-established mean spherical approximation methodology.

This assumes that surface-charged micelles interact through a screened electrostatic potential, as described elsewhere [21].

The structural parameters R_{par}, ν, σ, ρ_{pol}, and alfa (alfa= ionization coefficient of the micelle) are then obtained through the fitting of the product of $P(q)$ and $S(q)$ in Eq. (1) to the experimental data [20]. In the case of non-interacting micelles, $S(q)=1$ in Eq. (1). In our case, we made use of the Global fitting procedure (GENFIT software) [22–26] that performs a χ^2 minimization process by changing the free parameters until χ^2 reaches a minimum value. It allows the linkage among different fitting parameters from distinct scattering curves. This process improves the uniqueness of the final solution.

Surface tension measurements

The surface tension measurements were performed for Tween-20 solutions in the absence of salt and in the presence of NaSCN 0.10 mol L^{-1}, NaSCN 1.0 mol L^{-1}, NaCl 1.0 mol L^{-1}, NaSCN 1.0 mol L^{-1}, and NaF 1.0 mol L^{-1}, using an automatic Krüss K100 tensiometer (Krüss GmbH, Germany) and DuNoyu ring at 22.0±0.5 °C. All glass vials were carefully rinsed with piranha solution and Milli-Q water prior to the surface tension measurements. In order to be sure that the vials were really clean, the surface tension of Milli-Q water was always measured prior to the samples. All data represent mean values of triplicates. The surface excess (Γ) or the number of moles of solute molecules adsorbed at the liquid-air interface, per unit area, was calculated using the Gibbs adsorption isotherm:

$$\Gamma = -(1/RT)\,(\partial\gamma/\partial \ln c)_{T,P} \quad (2)$$

where R is the gas constant and T is the reciprocal of Γ yielded the area (A) occupied per mole of Tween-20 at the liquid-air interface.

Results and discussion

Particle characterization

PMMA/Tween-20 particles presented mean diameter D of (138±5) nm and ζ-potential of−(35±1) mV. In the emulsion polymerization process, the hydrophobic monomers form droplets in water and the surfactant acts as emulsifier. The monomers can be found in the droplets, in the micelles core or in the aqueous phase. The initiator reacts with the monomer in the aqueous phase, transferring the radical to the monomer. Still in aqueous phase, the monomer radical reacts with another monomer, forming a dimer radical, which reacts with another monomer successively until oligoradicals are formed. Due to its low solubility in water, the oligoradicals diffuse to the micelle cores, where the monomer concentration is much higher than in the aqueous phase, allowing chain propagation. One should note that in this process, the initiator remains covalently attached to the polymer end chain. Considering the mechanism described above [13], PMMA chains are expected to grow inside the Tween-20 hydrophobic cores. Therefore, the resulting particles surfaces must be enriched by polar poly(ethylene glycol) sorbitan and by sulfate groups stemming from polymerization initiator, which cause ζ-potential of−(41±1) mV.

Figure 1a shows a typical SEM image obtained for dried PMMA/Tween-20 particles, where 650 spherical particles (marked with red circles) were used to estimate the mean diameter as (182±6) nm. SEM images show connections among the particles, which can be generated by capillary

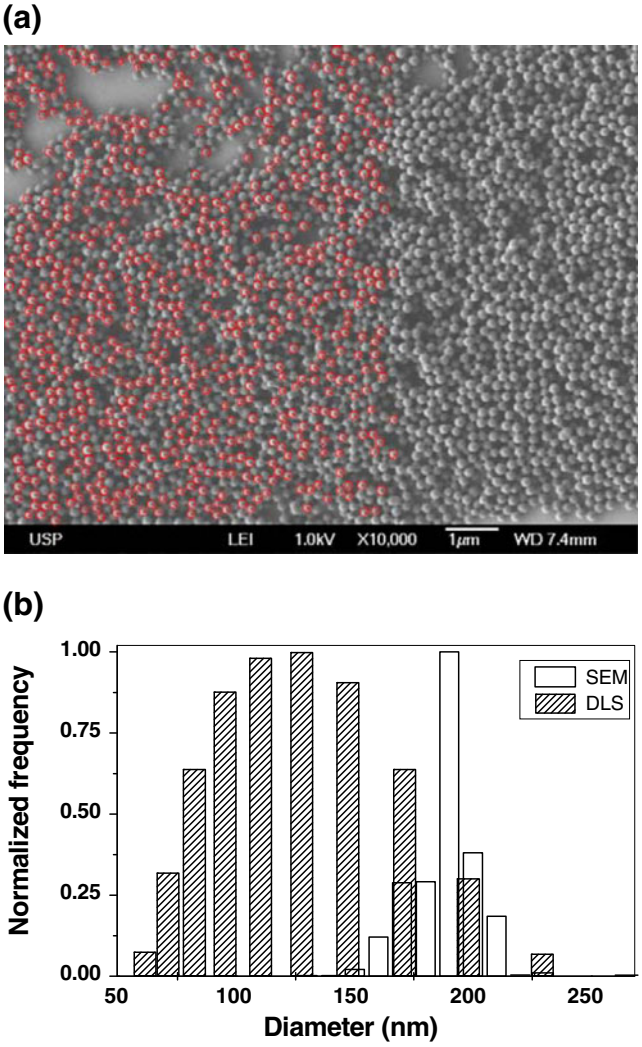

Fig. 1 **a** Typical scanning electron micrograph obtained for PMMA/Tween-20 particles after drying in the air. The *red circles* indicate the particles used for the diameter determination. **b** Normalized frequency of the diameter distribution determined by SEM (*open bars*) and DLS (*patterned bars*)

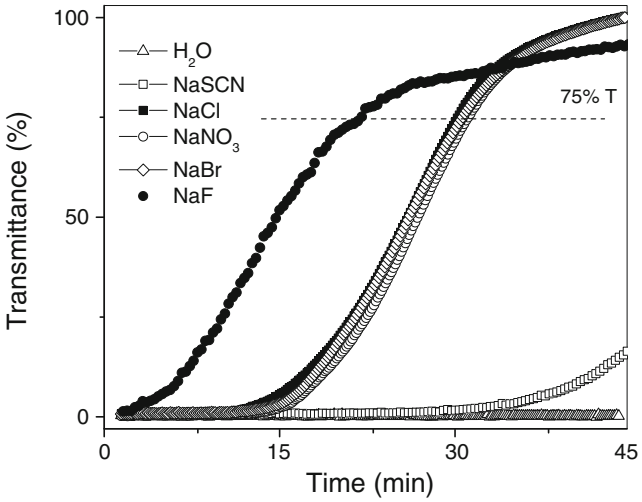

Fig. 2 Normalized integral light transmission determined as a function of time at (30±2) °C for aqueous PMMA/Tween-20 dispersions (N_P= 2.7 10^{12} particles mL^{-1}) in the absence (H_2O) and in the presence of NaF, NaCl, NaBr, $NaNO_3$, and NaSCN (1.00 mol L^{-1}). As a control experiment the transmittance at 75 %

forces during the coalescence process, since isolated particles have smooth surfaces. The particle diameter distribution determined by DLS and SEM is presented in Fig. 1b. The former indicated broader size distribution and smaller particles than the latter. One should notice that such differences are probably due to different sample preparation and measuring conditions. Dispersion solid content, polymerization yield, and N_P values amounted to 33±1 gL^{-1}, 52± 2 %, and (2.7±0.2) 10^{13} particles mL^{-1}, respectively.

Colloidal stability

Dialyzed PMMA/Tween-20 dispersions (N_P=2.7 10^{12} particles mL^{-1}) are stable over at least 6 months under room conditions (T=23±2 °C and 1 atm). The high stability is due to electrostatic repulsion caused by the ζ-potential of−(35±1) mV and by the highly hydrated poly(ethylene glycol) layer [27] on the particle surface, which provides "hydro-steric" repulsion [14].

The first set of colloidal stability experiments aimed to compare the colloidal stability of PMMA/Tween-20 particles with that of commercial polystyrene sulfate (PSS, Interfacial Dynamics Corp Portland, USA) latex particles with mean diameter of 85 nm and ζ-potential of −40 mV (in water), both at 2.0×10^{12} particles mL^{-1}. As observed in a previous work [13], in the presence of 0.3 mol L^{-1} NaCl, the PSS particles precipitated immediately. However, PMMA/Tween-20 particles were visually stable over 1 day, indicating that the colloidal stability is due to the presence of negative charges and to the steric repulsion caused by the whole hydrated PEG "hairy layer" on the particles surface.

In the second set of experiments, the colloidal stability of PMMA/Tween-20 particles in the presence of monovalent Hofmeister anions was investigated. Figure 2 shows the phase separation behavior of PMMA/Tween-20 dispersions in the presence of NaF, NaCl, NaBr, $NaNO_3$, and NaSCN. One can observe three different behaviors, namely, a fast, a slow, and an intermediate phase separation. Table 1 shows the time necessary to achieve the transmittance level of 75 %, which was arbitrarily chosen for the sake of comparison, in the presence of each salt. For comparison, the transmittance determined for PMMA/Tween-20 in pure water as a function of time was also presented. The system destabilized faster in the presence of NaF (1,240±140 s), while in the presence of NaSCN, it took 3,720±150 s. Intermediate times close to 1,700 s were observed for dispersions in the presence of NaCl, NaBr, and $NaNO_3$. The effect of these anions on the colloidal stability of PMMA/Tween-20 dispersions followed the same order of the Hofmeister series. It can be observed that the most chaotropic anions, which are also the least hydrated, are the slowest to cause aggregation, while the kosmotropes, which are the more hydrated, are the fastest ones. The phase separation behavior observed might be a consequence of the changes caused by the anion on the hydration layer of the particles, but also by interactions between the hydrated ion and the Tween-20 polar poly (ethylene glycol) segments on the particle surfaces. A similar behavior was observed for poly(N-isopropylacrylamide-co-dimethyl aminoethylmethacrylate) microgel latexes, which were deswollen in a more pronounced way in the presence of citrate than in the presence of SCN^- [28].

The correlation between the anions' ability to destabilize the PMMA/Tween-20 dispersions and the Hofmeister ions

Table 1 Time necessary to destabilize original PMMA/Tween-20 particles at N_P=2.7 10^{12} particles mL^{-1} in the presence of sodium salts at 1.00 mol L^{-1} and re-dispersed particles determined at (30±2) °C, along with the corresponding anion hydration enthalpy (ΔH_{hyd})

Anions (Na^+ as counter-ion)					
	F^-	Cl^-	Br^-	NO_3^-	SCN^-
Time (s)	1,240±140	1,680±50	1,700±85	1,750±135	3,720±150
Time (s), re-dispersed	1,460±100	2,400±55	2,460±60	2,540±140	4,510±85
Anion ΔH_{hyd} (kJ mol^{-1})	−520	−390	−360	−295	−310

For the sake of comparison, the transmittance level of 75 % was considered for all systems

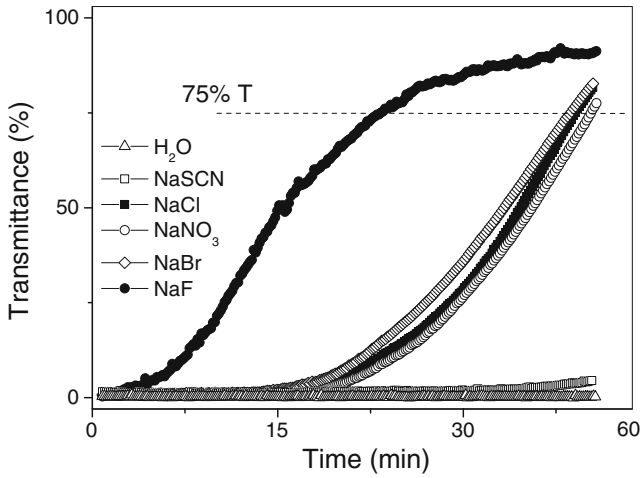

Fig. 3 Normalized integral light transmission determined as a function of time at (30±2) °C for re-dispersed PMMA/Tween-20 (N_P=2.7 10^{12} particles mL^{-1}) particles in the absence (H_2O) and in the presence of NaF, NaCl, NaBr, $NaNO_3$, and NaSCN (1.00 mol L^{-1}). The *dashed line* represents the level of transmittance at 75 %

series might be explained by specific interaction between the PEG oligomers on the particle surface and anions. For instance, in the effectiveness of sodium salts in salting-out aqueous solution of an 8,000 g mol^{-1} poly(ethylene)glycol followed the Hofmeister anions series [29]. The cloud-points of poly(ethylene)glycol-based surfactant solutions are also affected by the type of the ions. Kosmotropes, which exert high electric field at short distance, compete for water around PEG chains, leading to dehydration [28] and cloud-point depression. Conversely, chaotrope ions exert weak electric field, promote PEG chains hydration, and increase the cloud-points [28–35]. Micelles of triblock copolymer of ethylene oxide and propylene oxide (Pluronic 123) self-assembled in a wormlike shape in the presence of F^-, a kosmotrope, due to dehydration of polyethylene glycol chains in the micelles corona [36]. Thus, NaF caused the fastest phase separation because it was the most efficient to dehydrate PEG oligomers on PMMA/Tween-20 particles.

The aggregation of PMMA/Tween-20 particles in the presence of salts was reversible and re-dispersion into a homogeneous system was achieved by manual shaking. The phase separation of all systems immediately measured after re-dispersion is shown in Fig. 3 and the time necessary to achieve the transmittance level of 75 % in the presence of each salt is presented in Table 1. In the presence of NaF, the time need to destabilize the re-dispersed particles was similar to that observed originally, considering the standard errors. In the case of NaCl, NaBr, and $NaNO_3$, the time need to destabilize the re-dispersed particles increased ~45 %, while in the presence of NaSCN, it increased ~20 %. These findings evidence that the re-dispersed particles differ from the original ones, except for the dispersions in the presence of NaF. Changes observed in the presence of NaCl, NaBr, $NaNO_3$, and NaSCN might be associated to the adsorption of ions on the hydrophilic shell of PEG oligomers. If some anions adsorbed onto the PEG oligomers, the surface charge increased and electrostatic repulsion might be responsible for the increase in the time necessary to destabilize the dispersion. Following this rationale, the adsorption of SCN^- on PEG should be larger than that of Cl^-, Br^-, or NO_3^-. As a control experiment, the transmittance was also determined for PMMA/Tween-20 in pure water.

In order to gain insight about the interactions between the anions and PMMA/Tween-20 particles at molecular level, micelles of Tween-20 were used to mimic the particles. The small size of micelles compared to the particles allows exploring the effects of ions on the outmost PEG layer by means of SAXS and surface tension measurements.

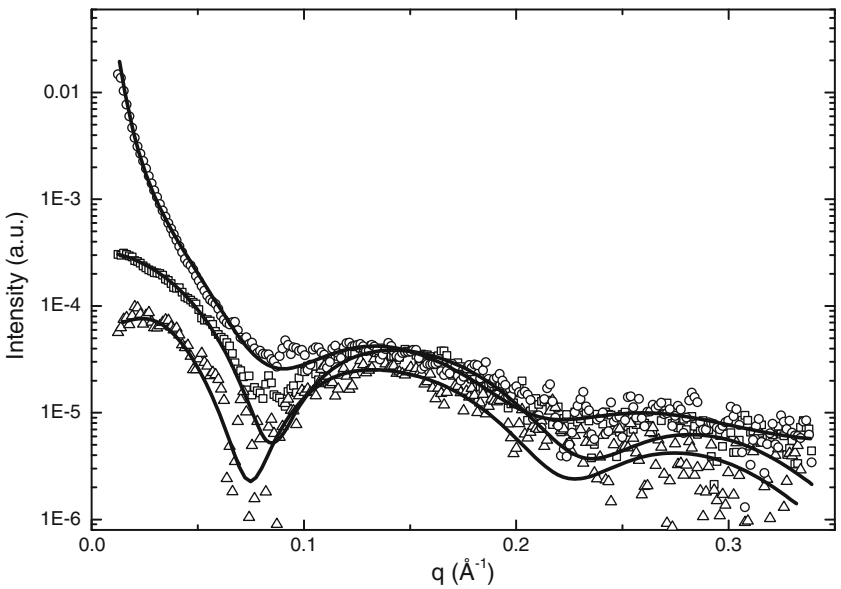

Fig. 4 Experimental scattering curves obtained for Tween-20 at 1.0 mmol L^{-1} in the absence (*open squares*) and presence of NaSCN 1.0 mol L^{-1} (*open triangles*) and NaF 1.0 mol L^{-1} (*open circles*) along with the best fitting (*solid lines*) to the experimental data. The fitting parameters are displayed on Table 2

Table 2 Fitting parameters obtained from the analysis of the micelle form factor *P*(q) determined from SAXS curves in Fig. 4

System	R_{par} (Å)	σ_{pol} (Å)	ρ_{pol} (e/Å^3)	ν
Tween-20	20.6±0.5	8.4±0.5	0.40±0.01	1.95±0.05
Tween-20 + NaSCN 1.0 mol.L^{-1}	19.4±0.7	10.5±0.5	0.42±0.01	2.1±0.1
Tween-20 + NaF 1.0 mol.L^{-1}	20.6±0.5	11.8±0.5	0.39±0.01	2.8±0.1

Figure 4 shows the experimental scattering curves obtained for Tween-20 at 1.0 mmol L^{-1} in the absence (open squares) and presence of NaSCN 1.0 mol L^{-1} (open triangles) and NaF 1.0 mol L^{-1} (open circles) along with the best fitting (solid lines) to the experimental data. Tween-20 scattering curve exhibits a broad peak at q ~0.14 Å^{-1}, which is characteristic of micelle-like aggregates in solution [21]. The quality of the fitting to the data is rather good, indicating that the scattering of the Tween-20 micelle-like aggregate is well represented by the scattering of a small prolate ellipsoid with an inner hydrophobic core (the smallest and longest semi-axes of circa 21 Å and 40 Å , respectively) surrounded by a 8.5-Å thick polar shell (Table 2). For comparison, fluorescence correlation spectroscopy data obtained for Tween-20 yielded hydrodynamic radius of 29 ±1 Å [37]. The model used to analyze the scattering data suggests that the micelles resemble small prolate ellipsoids in solution, the fitting parameters are displayed on Table 2. Tween-20 micelles were also analyzed by means of DLS and ζ-potential measurements. The mean hydrodynamic radius and ζ-potential value amounted to 37±2 Å and of− (9±1) mV, respectively. These values might be overestimated, because they were calculated considering Tween-20 micelles as spheres, which do not correspond to their real form (prolate ellipsoid). Comparing the ζ-potential values determined for PMMA/Tween-20 (−35 mV) with that found for Tween-20 micelles (−9 mV), one can conclude that the sulfate groups stemming from initiator contribute significantly to the surface potential on the polymer particles.

Upon addition of NaSCN, another peak at lower q range (q ~0.025 Å^{-1}) appeared. Such peak in the scattering curve is typical of a system containing surface-charged micelles interacting through a repulsive electrostatic potential [21, 38]. In this way, the scattering curve was modeled by a product of *P*(q) and *S*(q) (Eq. 1), as described in the Experimental Section. The *P*(q) results indicate that the presence of NaSCN in the solution does not cause a significant impact on micelle structural features, see Table 2. On the other hand, it is possible to infer that the SCN^- ions must reside on the polar shell, since its thickness and electron density increased in respect to the ion-free micelles (Table 2). Furthermore, a micelle ionization coefficient of 20 % was found from the analysis of the *S*(q) function. One should bear in mind, however, that this is an effective value and it can take into account some of the deficient of the model [21] Therefore, the SAXS result evidences that SCN^- ions are located preferentially on the micelles surface, interacting with polar headgroups. Such a preferential ion location gives rise to new surface-charged micelles and corroborates with the phase separation behavior observed in Figs. 2 and 3, which showed that the time required to destabilize the PMMA/Tween-20 dispersions was the longest in the presence of SCN^- ions.

The presence of NaF promotes different changes on Tween-20 micelles. There is a huge increase in the scattering at low q values (Fig. 4) as compared to the SAXS data for micelles in the absence and presence of NaSCN (Fig. 4), indicating that large aggregates are formed under the influence of NaF ions. In this way, the SAXS curve obtained for Tween-20 in the presence of NaF was fitted considering the presence of micelles, evidenced by the broad peak at q ~0.14 Å^{-1}, and of large aggregates (Porod´s law, *I*(q) is proportional to q^{-4}) [17, 19], revealed by the large intensity at very low q values. The shape and the size of such large aggregates could not be determined due to the limited resolution in this q range. On the other hand, the *P*(q) fitting parameters shown in Table 2 show that NaF induced significant changes in the dimensions of Tween-20 micelles. The anisometry (ν) of the ellipsoid-like micelle increased from circa 2 to 2.8 and the polar shell thickness σ_{pol} values increased from 8.5 to 12 Å, without affecting the polar electron density. The R_{par} values did not change, evidencing

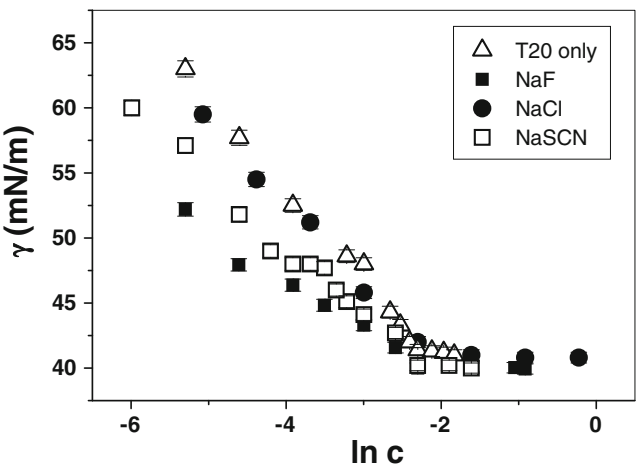

Fig. 5 Surface tension measurements as a function of ln Tween-20 concentration determined for Tween-20 solutions in the absence (*open triangles*) and in the presence of NaF 1.0 mol L^{-1} (*solid squares*), NaCl 1.0 mol L^{-1} (*solid circles*) or NaSCN 1.0 mol L^{-1} (*open squares*) at (22.0±0.5) °C

Table 3 Calculated values of ($\partial\gamma$ / ∂ln c), surface excess (Γ), and the area (A) occupied per Tween-20 molecule at the liquid–air interface at (22±1) °C

System	($\partial\gamma$ / ∂ln c) (mN m^{-1})	Γ (10^{17} molecules/m²)	A (Å²/molecule)
Tween-20	−6.98±0.07	17.1±0.2	58±1
Tween-20 + NaCl 1.0 mol L^{-1}	−6.31±0.05	15.5±0.2	65±1
Tween-20 + NaSCN 1.0 mol L^{-1}	−5.19±0.05	12.7±0.1	78±1
Tween-20 + NaF 1.0 mol L^{-1}	−3.76±0.03	9.2±0.1	109±2

The figures are mean values with the corresponding standard errors determined from triplicates

that the effects are mainly on the micelle polar shell. These features and the appearance of longer structures (longest semi-axis of 70 Å) indicate that F^- ions induced the assembling of Tween-20 micelles, forming small coacervates. Concerning the large aggregates, those should have been formed due to the dehydration of PEG polar head, which promoted the collapse of many micelles. Fluoride ions favor the interactions with water molecules, leading to "salting-out" effect. A similar behavior was observed for the swelling and deswelling of gels made of poly(ethylene glycol) [39], hydroxypropylmethylcellulose [40] or poly(vinyl alcohol) [41] in the presence of Hofmeister anions. The general trend is that kosmotropic ions, like F^-, dehydrate the gels, while chaotropic ions, like SCN^-, favor gel swelling.

Surface tension measurements were performed for Tween-20 in pure water and in the presence of NaF, NaCl, and NaSCN, 1.0 mol L^{-1} each, as shown in Fig. 5. The c.m.c. and the surface tension value at the c.m.c. for Tween-20 in pure water amounted to 0.10±0.01 mmol L^{-1} and 41±1 mN/m, respectively, which are in agreement with literature data [42]. These values were not affected by the presence of any salt. On the other hand, the Γ values and, consequently, the surface area (A) per Tween-20 molecule at the liquid–air interface were affected by the presence of anions, as presented in Table 3. The calculated A values increased from 58±1 Å² for pure Tween-20 solutions to 65±1 Å², 78±1 Å², and 109±2 Å² due to the presence of 1.0 mol L^{-1} Cl^-, SCN^-. and F^- anions, respectively. These findings indicate that Cl^- and SCN^- ions interact with the Tween-20 headgroup, but at different extent, corroborating with results reported for other self-assembled amphiphilic molecules [43, 44]. Regarding the effects of Cl^- and SCN^- ions, molecular dynamics simulations were performed for palmitoyloleoylphosphatidylcholine bilayers in the fluid phase solvated by 1.0 mol L^{-1} salt, which indicated that large chaotropes like SCN^- penetrate deeper into the bilayer than do the Cl^- anions [43]. The effect of Hofmeister salts on the structure of 1,2-dipalmitoyl phosphatidylcholine (DPPC) Langmuir films at the air/salt solution interface was investigated by means of surface pressure–area isotherms, Brewster angle microscopy, grazing incidence X-ray diffraction, and infrared reflection–absorption spectroscopy [36]. All

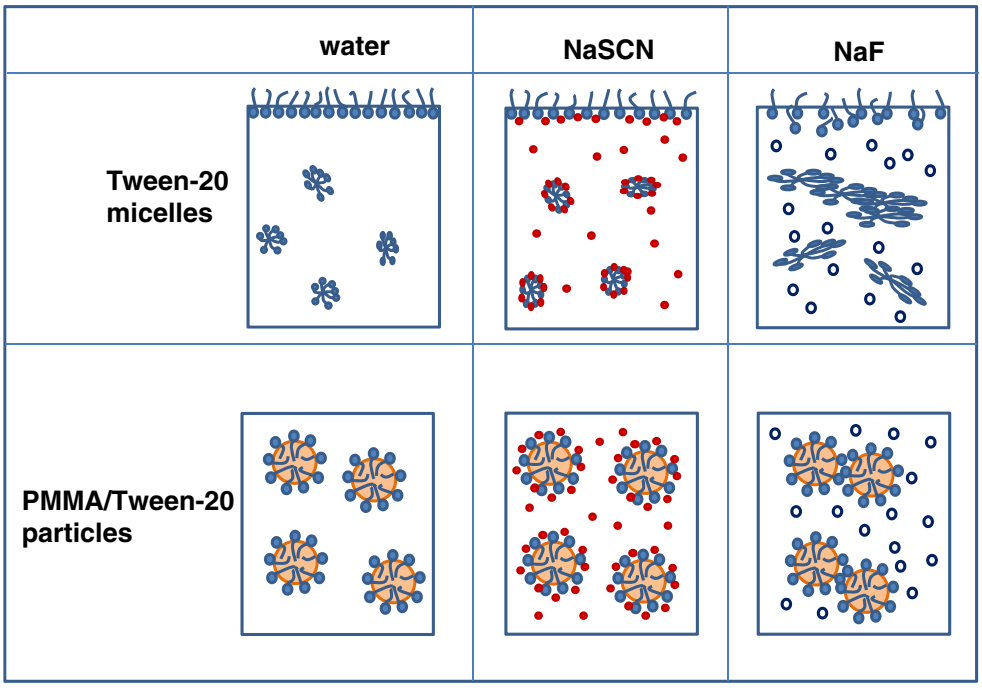

Fig. 6 Schematic representation of Tween-20 micelles and PMMA/Tween-20 particles in water, SCN^-, and F^- solution. The adsorption of SCN^- ions (*red circles*) onto the polar shell creates a new surface with higher charge density. The presence of F^- ions (*empty circles*) favors the dehydration of polar shell on PMMA/Tween-20 particles and Tween-20 micelles, destabilizing the systems. Tween-20 micelles and PMMA/Tween-20 particles are not to scale

anions increased the surface pressure at a given area per molecule. However, chaotropes led to larger increase in the surface pressures, because they penetrate deeper into the monolayer. Large anions like SCN^- tend to be more hydrophobic and to present relative large polarizability. For instance, iodide penetrated into the hydrophobic region of the DPPC monolayer and disturbed the packing properties [44]. The hydrophobic character might be correlated with the enthalpy of hydration (ΔH_{hyd}) values, which for iodine and SCN^- ions amount to −320 and −310 kJ mol^{-1}, respectively. In the case of Tween-20 micelles, SAXS data do not evidence penetration of SCN^- ions inside the micelle hydrophobic core, but they indicate the enrichment of micelle shells by negative charges (Table 2), which corroborate with the increase of *A* values (Table 3) and explain the longer times for phase separation of PMMA/Tween-20 particles in the presence of SCN^- ions, especially after re-dispersion of particles (Fig. 3). Contrary to the SCN^- ions, F^- ions are strongly hydrated and repelled from the air–water interface [45]. Thus, the large increase of *A* values (~88 %) in the presence of F^- ions probably reflects the presence of small coacervates of Tween-20 micelles adsorbed at the liquid–air interface, as indicates by SAXS data.

The effect of ions on the *A* values did not follow the order of the Hofmeister series. *A* possible explanation might be that while F^- ions favor Tween micellization by "salting-out", less Tween adsorbs to the liquid–air interface. NaSCN ions, on the other extreme, adsorb to the Tween molecules, causing their mutual repulsion—again increasing the area per Tween molecule at the surface. NaCl is least effective both in "salting-out" and in adsorption onto Tween, hence it has lowest effect on the tensiometry results compared to Tween in pure water.

Conclusions

The phase separation behavior of PMMA/Tween-20 dispersions in the presence of NaF, NaCl, NaBr, $NaNO_3$, and NaSCN followed the same order of the Hofmeister series. Except for F^- ions, the adsorption of anions onto the PEG outmost layer (of polymer particles or micelles) was evidenced by the increase in (a) the time necessary to destabilize a re-dispersed system and (b) the thickness of polar shell of Tween-20 micelles. These effects increased with the increase of ion polarizability [4], size, and enthalpy of hydration. Fluoride ions did not adsorb on the external PEG shell (of polymer particles or micelles), but they caused its dehydration and, consequently, destabilized the systems. Based on the experimental data, a model was proposed (Fig. 6), where Tween-20 micelles and PMMA/Tween-20 particles are represented in water, SCN^-, and F^- solution. The SCN^- ions (chaotropes) are not strongly bound to their hydrating layer, favoring their adsorption onto the PEG shell and, consequently, promoting the creation of a new surface with higher charge density. The F^- ions (kosmotropes) bind strongly to their hydration layer, favoring their own hydration. Consequently, the polar shell on PMMA/Tween-20 particles and Tween-20 micelles might undergo dehydration, destabilizing the systems. Considering the potential applications PEG-decorated particles, such as PMMA/Tween-20 particles, in biotechnological processes, these results are of fundamental relevance for the adequate choice of electrolytes to be used upon designing formulations and diagnostic kits, where the colloidal stability is a primary requirement.

Acknowledgments The authors thank CNPq, CAPES and FAPESP (Grant # 2010/51219-4) for financial support. J.O.S. thanks Pró-Reitoria de Graduação da Universidade de São Paulo for the undergraduate stipend. The authors are also in debt with Prof. Paolo Mariani and Franceco Spinozzi, both from Università Politecnica delle Marche, Ancona, Italy, who provided us the GENFIT software.

References

1. Hofmeister F (1888) Zur Lehre von der Wirkung der Salze. Arch Exp Pathol Pharmakol 24:247–260
2. Cacace MG, Landau EM, Ramsden JJ (1997) The Hofmeister series: salt and solvent effects on interfacial phenomena. Quat Rev Biophys 30:241–277
3. Leontidis E (2002) Monolayers, bilayers and micelles of zwitterionic lipids as model systems for the study of specific anion effects. Curr Opin Colloid Interface Sci 7:81–91
4. Kunz W, Lo Nostro P, Ninham BW (2004) The present state of affairs with Hofmeister effects. Curr Opin Colloid Interface Sci 9:1–18
5. Zhang Y, Cremer PS (2006) Interactions between macromolecules and ions: the Hofmeister series. Curr Opin Chem Biol 10:658–663
6. Zhang Y, Furyk S, Bergbreiter DE, Cremer PS (2005) Specific ion effects on the water solubility of macromolecules: PNIPAM and the Hofmeister series. J Am Chem Soc 127:14505–14510
7. Petrache HI, Zemb T, Belloni L, Parsegian VA (2006) Salt screening and specific ion adsorption determine neutral-lipid membrane interactions. Proc Natl Acad Sci 103:7982–7987
8. Santos AP, Levin Y (2011) Ion specificity and the theory of stability of colloidal suspensions. Phys Rev Lett PRL 106: 167801–167804
9. Manciu M, Ruckenstein E (2007) On possible microscopic origins of the swelling of neutral lipid bilayers induced by simple salts. J Colloid Interface Sci 309:56–67
10. Bonfá A, Saito RSN, França RFO, Fonseca BAL, Petri DFS (2011) Poly(ethylene glycol) decorated poly(methylmethacrylate) nanoparticles for protein adsorption. Mater Sci Eng C Biomim Mater Sensors Syst 31:562–566
11. Lövgren U, Johansson M, Kronkvist K, Edholm LE (1995) Biocompatible sample pretreatment for immunochemical techniques using micellar liquid-chromatography for separation of corticosteroids. J Chromatogr B Biomed Sci Appl 672:33–44
12. Zana R (2005) Dynamics in micellar solutions of amphiphilic block copolymers. In: Zana R (ed) Dynamics of surfactant self-assemblies. CRC, Taylor & Francis Group, New York, pp 161–231

13. Gilbert R (1995) Emulsion polymerization: a mechanistic approach. Academic Press, London
14. Correia FM, Petri DFS, Carmona-Ribeiro AM (2004) Colloidal stability of lipid/polyelectrolyte decorated latex. Langmuir 20:9535–9540
15. Reis EAO, Caraschi JC, Carmona-Ribeiro AM, Petri DFS (2003) Polyelectrolytes at charged particles: particle number density, molecular weight and charge ratio effects. J Phys Chem B 107:7993–7997
16. Castro LBR, Soares KV, Naves AF, Carmona-Ribeiro AM, Petri DFS (2004) Synthesis of stable polystyrene and poly(methyl methacrylate) particles in the presence of caboxymethyl cellulose. Ind Eng Chem Res 43:7774–7779
17. Guinier A, Fournet G (1955) Small angle scattering of X-Rays. Wiley, New York
18. Svergun DI, Feigin LA (1987) Structure analysis by small-angle X-ray and Neutron scattering. Plenum, New York
19. Glatter O, Kratky O (1982) Small angle X-ray scattering. Academic Press, New York
20. Marignan J, Basserau DP (1986) Effect of pentanol and concentration on the micelles in the system OBS/water/1-pentanol. J Phys Chem 90:645–652
21. Barbosa LRS, Caetano W, Itri R, Homem-De-Mello P, Santiago PS, Tabak M (2006) Interaction of phenothiazine compounds with zwitterionic lysophosphatidylcholine micelles: small angle x-ray scattering, electronic absorption spectroscopy, and theoretical calculations. J Phys Chem B 110:13086–13093
22. Sinibaldi R, Ortore MG, Mariani P (2007) Preferential hydration of lysozyme in water/glycerol mixtures: a small-angle neutron scattering study. J Chem Phys 126:235101–235110
23. Sinibaldi R, Ortore MG, Spinozzi F, Funari SS, Teixeira J, Mariani P (2008) SANS/SAXS study of the BSA solvation properties in aqueous urea solutions via a global fit approach. Eur Biophys J 37:673–681
24. Barbosa LRS, Ortore MG, Spinozzi F, Mariani P, Bernstorff S, Itri R (2010) The importance of protein–protein interactions on the pH-induced conformational changes of bovine serum albumin: a small-angle X-ray scattering study. Biophys J 98:147–157
25. Barbosa LRS, Rigos CF, Yoneda JS, Itri R, Ciancaglini P (2010) Unraveling the Na, K-ATPase alpha(4) subunit assembling induced by large amounts of C(12)E(8) by means of small-angle X-ray scattering. J Phys Chem B 114:11371–11376
26. Press WH, Teukolsky SA, Flannery BP (1994) Numerical recipes: the art of scientific computing. Cambridge University Press, Cambridge
27. Anderson A, Ashurst WR (2009) interfacial water structure on a highly hydroxylated silica film. Langmuir 25:11549–11554
28. Zha L, Hu J, Wang C, Fu S, Luo M (2002) The effect of electrolyte on the colloidal properties of poly(N-isopropylacrylamide-co- dimethyl aminoethylmethacrylate) microgel latexes. Colloid Polym Sci 280:1116–1121
29. Hey MJ, Jackson DP, Yan H (2005) The salting-out effect and phase separation in aqueous solutions of electrolytes and poly (ethylene glycol). Polymer 46:2567–2572
30. Schott H, Royce AE, Han SK (1984) Effect of inorganic additives on solutions of nonionic surfactants. Cloud points shift values of the individual ions. J Colloid Interface Sci 98:196–201
31. Weckström K, Zulauf M (1985) Lower consolute boundaries of a poly(oxyethylene) surfactant in aqueous-solutions of monovalent salts. J Chem Soc Faraday Trans 81:2947–2958
32. Koshy L, Saiyad AH, Rakshit AK (1996) The effects of various foreign substances on the cloud point of Triton X 100 and Triton X 114. Colloid Polym Sci 274:582–587
33. Schott H (1997) Effect of inorganic additives on solutions of nonionic surfactants. Effect of chaotropic anions on the cloud point of octoxynol 9 (Triton X-100). J Colloid Interface Sci 189:117–122
34. Zheng LQ, Minamikawa H, Harada K, Inoue T, Chernik GG (2003) Effect of inorganic salts on the phase behavior of an aqueous mixture of heptaethylene glycol dodecyl ether. Langmuir 19:10487–10494
35. Bloksma MM, Bakker DJ, Weber C, Hoogenboom R, Schubert US (2010) The effect of Hofmeister salts on the LCST transition of poly(2-oxazoline)s with varying hydrophilicity. Macromol Rapid Commun 31:724–728
36. Denkova AG, Mendes E, Coppens MO (2008) Effects of salts and ethanol on the population and morphology of triblock copolymer micelles in solution. J Phys Chem B 112:793–801
37. Luschtinetz F, Dosche C (2009) Determination of micelle diffusion coefficients with fluorescence correlation spectroscopy (FCS). J Colloid Interface Sci 338:312–315
38. Barbosa LRS, Itri R, Tabak M, Caetano W (2003) Trifluoperazine effects on anionic and zwitterionic micelles: a study by small angle X-ray scattering. J Colloid Interface Sci 260:414–422
39. Masuda Y, Nakanishi T (2002) Ion-specific swelling behavior of poly(ethylene oxide) gel and the correlation to the intrinsic viscosity of the polymer in salt solutions. Colloid Polym Sci 280:547–553
40. Liu SQ, Joshi SC, Lam YC (2008) Effects of salts in the Hofmeister series and solvent isotopes on the gelation mechanisms for hydroxypropylmethylcellulose hydrogels. J Appl Polym Sci 109:363–372
41. Masuda Y, Tanaka T, Nakanishi T (2001) Ion-specific swelling behavior of poly(vinyl alcohol) gel prepared by gamma-ray irradiation. Colloid Polym Sci 279:1241–1244
42. Samanta S, Ghosh P (2011) Coalescence of bubbles and stability of foams in aqueous solutions of Tween surfactants. Chem Eng Res Des 89:2344–2355
43. Sachs JN, Woolf TB (2003) Understanding the Hofmeister effect in interactions between chaotropic anions and lipid bilayers: molecular dynamics simulations. J Am Chem Soc 125:8742–8743
44. Aroti A, Leontidis E, Maltseva E, Brezesinski G (2004) Effects of Hofmeister anions on DPPC Langmuir monolayers at the air–water interface. J Phys Chem B 108:15238–15245
45. Santos AP, Diehl A, Levin Y (2010) Surface tensions, surface potentials, and the Hofmeister series of electrolyte solutions. Langmuir 26:10778–10783